# CO adsorption on metal surfaces: A hybrid functional study with plane-wave basis set

Alessandro Stroppa,* Konstantinos Termentzidis, Joachim Paier, Georg Kresse, and Jürgen Hafner
*Faculty of Physics, Universität Wien, and Center for Computational Materials Science, Sensengasse 8/12, A-1090 Wien, Austria*
(Received 23 June 2007; revised manuscript received 21 September 2007; published 27 November 2007)

We present a detailed study of the adsorption of CO on Cu, Rh, and Pt (111) surfaces in top and hollow sites. The study has been performed using the local density approximation, the gradient corrected functional PBE, and the hybrid Hartree-Fock density functionals PBE0 and HSE03 within the framework of generalized Kohn-Sham density functional theory using a plane-wave basis set. As expected, the local density approximation and generalized gradient approximation functionals show a tendency to favor the hollow sites, at variance with experimental findings that give the top site as the most stable adsorption site. The PBE0 and HSE03 functionals reduce this tendency. In fact, they predict the correct adsorption site for Cu and Rh but fail for Pt. However, even in this case, the hybrid functional destabilizes the hollow site by 50 meV compared to the PBE functional. The results of the total energy calculations are presented along with an analysis of the projected density of states.

DOI: 10.1103/PhysRevB.76.195440 PACS number(s): 68.43.Bc, 68.47.De, 71.15.Mb

## I. INTRODUCTION

The adsorption of carbon monoxide on metal surfaces is an important case study in surface science for two reasons. On one hand, the interaction of CO with metal surfaces plays a major role in understanding phenomena related to, e.g., catalysis, adhesion, and coating as well as in many industrial processes, such as automotive catalysis, corrosion, tribology, and gas sensing.[1] Catalysts containing transition metals, such as rhodium, palladium, and platinum, have been widely used to lower the emissions of CO in automobile exhausts.[1] For all the mentioned applications, it is clear that understanding adsorption on both bare and adsorbate-covered surfaces is an important issue.

On the other hand, the failure of density functional theory (DFT) based on local and semilocal density functionals in predicting the correct adsorption site for CO on metal surfaces is well known. The most notable example in literature is the CO/Pt(111) system, often referred to as *CO adsorption puzzle*. No "stone was left unturned"[2] in order to determine the reason for the discrepancy between theory and experiment, but neither defect structures and contaminations, relativistic or spin effects, nor zero-point energies can account for the difference: there is strong evidence that current approximations to DFT underestimate the CO preference for low-coordination sites.[2,3] Most plane-wave codes predict that the hollow site is preferred for CO on Cu, Rh, and Pt (with the exception of Ref. 4 for CO on Rh), whereas experimentally it is found that CO adsorbs at the top site with the carbon end down at low coverage on all three substrates.[5–8] In all fairness, it must be emphasized that some local basis-set codes (specifically DMOL and ADF) seem to give the proper site order for Pt.[9,10] The reason for the discrepancy between local basis-set codes and plane-wave codes is not yet entirely understood, but it is likely to be related to the different treatment of relativistic effects or basis sets. For Pt, the DMOL code, for instance, applies effective core potentials to take into account relativistic effects, and the site preference depends critically on the used effective core potential, with the most accurate effective core potential giving the same site preference as plane-wave codes.[11] The Amsterdam density functional code (ADF) also yields the correct site order for Pt.[10] Basis-set convergence, *k*-point sampling, as well as relativistic effects have been carefully checked for CO on Pt, and it is at this point unclear why results differ from those reported using plane waves.

Very recently, Hu *et al.*[12] have shown that errors of present-day exchange-correlation (xc) functionals are rather localized and spatially limited to few nearest neighbors. For extended systems, the *correction* can be estimated by analyzing properly chosen clusters and employing wave function based methods for an improved xc treatment. According to their study, this procedure applied to CO/Cu(111) and CO/Ag(111) gives the top site as the most stable adsorption site, in agreement with the experiments.[12] Returning to the discrepancy between theory and experiment obtained using DFT and plane waves, the current suggestion is that the main reason for the failure is due to the incorrect description of the relative position of the highest occupied molecular orbital (HOMO) and lowest unoccupied molecular orbital (LUMO) of CO with respect to the Fermi energy of the metal.[13] To overcome this problem, several possibilities have been considered so far. One is to apply an *a posteriori* correction, based on the singlet-triplet CO excitation energy obtained by GGA and configuration interaction calculations.[14] A second option is using a DFT+$U$ approach, where an additional $U$ is added to the DFT Hamiltonian to shift the CO LUMO to higher energies.[3,15] A third self-contained and less *ad hoc* approach is the use of hybrid functionals.[13]

Hybrid functionals are a combination of exact nonlocal orbital-dependent Hartree-Fock (HF) exchange and a standard local exchange-correlation functional, and they provide a significant improvement over the LDA-GGA description for molecular as well as extended insulating and semiconducting solid state systems.[16] For these systems, hybrid functionals are among the most accurate functionals available as far as energetics and structural properties are concerned.[17,18]

Currently, the most popular ones are PBE0 (or PBE1PBE)[19,20] and B3LYP.[21,22] The former has been proposed by Ernzerhof and co-workers[23,24] and Adamo and

 

Barone[20] as a "parameter-free" functional based on the PBE exchange-correlation functional. It has promising performance for all important properties, being competitive with the most reliable, empirically parametrized functionals.[20] The latter was suggested by Becke[21] and soon developed into the most popular and most widely used functional for quantum chemical calculations. This functional reproduces the thermochemical properties of atoms and molecules rather well.[25]

For periodic systems, in particular, metals, however, the long-range nature of the Fock exchange interaction and the resultant large computational requirements present a major drawback. Recently, a new hybrid functional, called HSE03, has been introduced by Heyd *et al.*[26] This functional addresses this problem by separating the description of the exchange interaction into a short- and a long-range part, where the long-range part is treated by semilocal gradient corrected functionals. The new functional yields a description of molecular properties comparable to the results obtained using the PBE0 functional and, in some cases, it even gives a slight improvement over the latter.[26]

To the best of our knowledge, very few *ab initio* calculations based on hybrid functionals have been concerned with the problem of CO adsorption on metal surfaces. Gil *et al.*[13] reported on the CO adsorption on the Pt(111) surface using both slabs and cluster models with local, semilocal, and hybrid functionals (B3LYP). However, the B3LYP calculations were restricted to clusters and extrapolation to large clusters seems to indicate that convergence with respect to the cluster size was not obtained. The B3LYP functional renders the on top and fcc sites almost degenerate, whereas LDA and GGA show a pronounced tendency to favor fcc adsorption. This was confirmed in the work of Doll[27] on the same system, where a careful comparison between gradient corrected functionals and the B3LYP functional has been reported. It was shown that the B3LYP functional gives the top site as the preferred site. Finally, in the work of Neef and Doll,[28] the adsorption of CO on the Cu(111) surface has been studied using the local density approximation, the gradient corrected functional of Perdew and Wang, and the B3LYP functional. The LDA and GGA yield the fcc site as favorable adsorption site, whereas the B3LYP functional results in the preference of the top site, in agreement with the experiment. The recent study for CO on Cu and Ag(111) came to similar conclusions.[12] All these hybrid functional studies applied only B3LYP and they made use of localized basis sets, which are possibly affected by basis-set superposition errors.

The aim of the present report is to present an extensive density functional study of the adsorption of CO on close-packed (111) metallic surfaces using the PBE0 and HSE03 functionals, which have not been considered yet for this specific problem. We also include, for comparison, the local density approximation and the standard gradient corrected PBE functional, which is widely accepted as the best parameter-free density functional available. We discuss in detail the application of these functionals to bulk and bare Cu, Rh, and Pt surfaces and the corresponding CO adsorption problem.

The study is pursued within the framework of the plane-wave projector-augmented-wave (PAW) formalism. Based on the approach of Chawla and Voth[29] for the evaluation of the exact exchange, PBE0 and HSE03 functionals have been recently implemented in the Vienna *ab initio* simulation package (VASP).[30] We remark that the use of a plane-wave basis set for the evaluation of the exact exchange energy allows for calculations that are free of basis-set superposition errors and benefit from the computational efficiency of fast Fourier transforms. Details of the implementation are given elsewhere.[16,31] We will focus on three reference metal systems, Cu, Rh, and Pt, which are among the best studied metallic surfaces concerning CO adsorption.[1] We note that the adsorption of CO on Rh(111) has not been investigated using hybrid functionals.

The paper is organized as follows. In the next section, we describe the computational approach and the model systems used. In Sec. III, we briefly review the calculated properties for the bulk and corresponding bare (111) surfaces as well as for the CO molecule. In Sec. IV, we discuss the results concerning the structural properties and energetics of the adsorbed CO molecule on the surface. Section V is devoted to the electronic properties in terms of density of states. In Sec. VI, we discuss the main results of this work, and in Sec. VII, we draw our conclusions.

## II. THEORETICAL AND COMPUTATIONAL METHOD

The first principles density functional theory calculations have been performed within the local and generalized gradient density approximations to DFT in the Ceperley-Alder and Perdew-Burke-Ernzerhof parametrization, respectively.[32,33] In the present calculations, the interaction between the ions and valence electrons is described by the PAW[34] method in the implementation of Kresse and Joubert.[35]

The cutoff energy has been fixed to 400 eV, which is sufficient to give well converged results for the systems considered in this work.[31] The surfaces have been modeled by a periodic four layer metal slab with a CO molecule adsorbed on one side of the slab, vertical to the (111) surface plane (asymmetric setup). For CO on Pt(111), tests with a six layer metal slab using the HSE03 functional have also been performed in order to check the convergence with respect to the slab thickness: the relative stability of the different sites does not change. Each slab is separated from its periodic image in the $z$ direction by a vacuum space of $\sim$10 Å. The two uppermost surface layers and the CO molecule are allowed to relax (substrate buckling up to the second layer below the surface). For the electronic relaxation, we fix the energy threshold to $10^{-3}$ eV, whereas the ionic relaxation is stopped when all forces are smaller than 0.1 eV/Å. We use a $c(2\times4)$ in-plane periodicity, which is equivalent to a coverage of $\Theta=0.25$ ML. With this choice, the separation between the molecule and its in-plane periodic images is large enough to neglect spurious adsorbate-adsorbate interactions with a reasonable computational effort.[36]

For the HSE03 calculations, the range separation parameter $\omega$ was set to $\omega=0.3$ Å$^{-1}$ in both the density functional part as well as the nonlocal Fock exchange.[37]

The Brillouin zone integrations are performed on symmetry reduced grids using the Monkhorst-Pack scheme.[38] To

TABLE I. Lattice constants $a_0$ (Å), bulk moduli $B_0$ (GPa), and cohesive energies $E_{coh}$ (eV) of bulk Cu, Rh, and Pt obtained from LDA, GGA (PBE), PBE0, and HSE03 calculations. Results for HSE03 are based on calculations employing a "reduced" $12\times12\times12$ $k$-point grid, and those for LDA, GGA (PBE), and PBE0 a full $12\times12\times12$ grid, i.e., without downsampling (see text for details). Relative errors (%) with respect to experiment are shown in parentheses.

| | $a_0$ (Å) | $B_0$ (GPa) | $E_{coh}$ (eV) |
|---|---|---|---|
| | | Cu | |
| LDA | 3.524 (−2.2%) | 184 (+29.0%) | 4.498 (+28.9%) |
| PBE | 3.635 (+0.9%) | 136 (−4.2%) | 3.484 (−0.2%) |
| PBE0 | 3.636 (+0.9%) | 130 (−8.4%) | 3.046 (−12.7%) |
| HSE03 | 3.640 (+1.0%) | 135 (−4.9%) | 3.066 (−12.1%) |
| B3LYP (Ref. 28) | 3.700 (+2.7%) | 117 (−17.6%) | 2.892 (−17.1%) |
| Expt. | 3.603 | 142 | 3.49 |
| | | Rh | |
| LDA | 3.752 (−1.2%) | 318 (+18.2%) | 7.382 (+28.4%) |
| PBE | 3.823 (+0.6%) | 254 (−5.6%) | 5.724 (−0.4%) |
| PBE0 | 3.785 (−0.3%) | 291 (+8.2%) | 4.205 (−26.9%) |
| HSE03 | 3.783 (−0.4%) | 305 (+13.4%) | 4.441 (−22.8%) |
| Expt. | 3.798 | 269 | 5.75 |
| | | Pt | |
| LDA | 3.905 (−0.4%) | 306 (+10.0%) | 7.076 (+20.9%) |
| PBE | 3.965 (+1.2%) | 277 (−0.4%) | 5.668 (−3.1%) |
| PBE0 | 3.932 (+0.3%) | 274 (−1.4%) | 4.648 (−20.5%) |
| HSE03 | 3.932 (+0.3%) | 275(−1.1%) | 4.900 (−16.2%) |
| B3LYP (Ref. 27) | 4.05 (+3.3%) | 234 (−15.8%) | 3.755 (−35.8%) |
| Expt. | 3.920 | 278 | 5.85 |

accelerate $k$-point convergence, we set the Methfessel-Paxton[39] smearing width to 0.1 eV. We have carefully checked the $k$-point convergence by performing calculations using $4\times4\times1$, $6\times6\times1$, and $8\times8\times1$ points (see discussion in Sec. IV). The numerical accuracy of the adsorption energies is estimated to be ~20 meV. We have also investigated the effect of downsampling the reciprocal space representation of the Fock exchange operator for the HSE03 functional as outlined in Ref. 31. In particular, the Fock exchange operator has been evaluated on the "full" $n\times n\times1$ $k$-point mesh, as well as on the corresponding "downsampled" $\frac{n}{2}\times\frac{n}{2}\times1$ grid, with $n$=4,6,8 (for details, see Ref. 31). Results are discussed in Sec. IV. Finally, we have also tested, for a reference case (HSE03), the effect of the parameter that controls the fast Fourier transformation (FFT) grid for the HF routines (keyword ENCUTFOCK in the VASP code). By considering the smallest possible FFT grid that just encloses the cutoff sphere corresponding to the plane-wave cutoff (ENCUTFOCK=0) or simply removing this constraint (without the flag ENCUTFOCK), total energies change by less than 5 meV.[40]

We considered three adsorption sites: top site, where CO is sitting vertically above a metal atom in the top layer, and the hcp (fcc) hollow site, where CO is sitting vertically above a metal atom in the second (third) topmost layer.

## III. BULK, BARE SURFACE, AND CO MOLECULE

Before studying the effect of CO adsorption on the (111) metal surfaces, we first consider the bulk and bare surfaces. In Table I, we summarize the results for the bulk systems reporting the lattice constant ($a_0$) and the bulk modulus ($B_0$) obtained using the Murnaghan equation of state. The cohesive energy ($E_{coh}$) is calculated considering unconstrained, i.e., spin polarized and nonspherical, ground states of the atoms.[16] The numbers in parentheses give the relative errors with respect to experiment.

As usual, the LDA (GGA) lattice constants are slightly underestimated (overestimated) with respect to the experiment. Note that the experimental lattice constants reported in Table I have not been extrapolated to 0 K and the zero-point quantum fluctuations have not been included in the DFT calculations. However, the inclusion of these contributions should change the values by only approximately ~0.1%, which we can neglect for the purpose of the present study.[41]

Using hybrid functionals, the lattice constant is almost unchanged for Cu (only a slight expansion is found using PBE0 and HSE03) and the overestimation is generally reduced in the other two cases. For Rh, the hybrid functionals overcorrect the lattice constant, giving a theoretical value smaller than the experimental one; for Pt, it remains slightly larger than experiments. Except for Cu, the agreement with

experiment improves using hybrid functionals (the PBE0 and HSE03 relative errors are smaller than the PBE ones).

The overestimation (underestimation) of the lattice constants goes in hand with an underestimation (overestimation) of the bulk moduli. The PBE functional predicts $B_0$ slightly more accurately than hybrid functionals for the systems under study.

The cohesive energies are overestimated at the LDA level, they are very well reproduced for the three bulk metals at the PBE level, but they are underestimated using hybrid functionals. The underbinding has been attributed to the admixture of Fock exchange and to the fact that Hartree-Fock usually underbinds, especially for metals.[27,42] We believe that this is not generally true for hybrid functionals. In fact, as shown in Ref. 31, the atomization energies for systems without $d$ electrons, such as Li, Na, and Al, are quite comparable for the PBE, PBE0, and HSE03 functionals (and very close to experimental results within 0.05–0.15 eV). Most probably, the reason for the reduction of the atomization energies of $d$ metals is related to the increased stability of the spin polarized atom compared with an artificial non-spin-polarized atom. The hybrid functional overestimates the exchange splitting in $d$ elements, with a consequent increase of the spin-polarization energy. This, however, does not explain the discrepancy for Cu. Here, we believe that the neglect of dynamical correlation effects between closed $d$ shells is a major source of errors accounting for roughly 210 meV of the discrepancy.[43] Proper inclusion of these van der Waals-like forces would also decrease the theoretical lattice constant of Cu.

For Cu and Pt, we can compare our hybrid functional results with Refs. 27 and 28, respectively. In Table I, it is evident that our results are significantly closer to the experiment than those of Refs. 27 and 28 at the bulk level. This is most likely related to the B3LYP functional being specifically designed for small molecules, limiting or reducing its precision for heavy elements.[44]

In Table II, we show the relevant properties of the bare surfaces: $d_{12}$ is the interlayer distance between the first and second topmost surface layers (and the corresponding relative variation with respect to the theoretical bulk value in parentheses) and the surface energies ($E_{surf}$).

For all functionals, the Cu and Rh surface layer relaxes inward. For Pt, the top layer relaxes outward. This "anomalous" relaxation is already documented in literature.[45,46] The change of $d_{12}$ relative to the theoretical interlayer bulk distance ($\Delta d_{12}$) for Cu is −0.9% using PBE, in agreement with calculations of Neef and Doll (PW91); the same quantity calculated using PBE0 (HSE03) is −1.8% (−0.9%), which is again close to the one obtained using B3LYP in the same work (−1.2%). For Rh, $\Delta d_{12}$ is −0.6% (PBE), −0.6% (PBE0), and −1.0% (HSE03), and for Pt, it is +0.7% (PBE), −1.3% (PBE0), and +1.3% (HSE03). Our values obtained both using standard GGA and hybrid functionals are slightly smaller than those obtained by Doll. The comparison with experiment is not simple due to the large uncertainties of the experimental values: for Cu $\Delta d_{12}$ is (−1.0±0.4)%,[47] for Rh it is (−1.3±0.9)%,[48] and for Pt it is (+1.1±0.4)%.[46] Agreement between our calculations and experimental results is certainly reasonable.

TABLE II. Relevant equilibrium properties of the bare surfaces using the LDA, GGA (PBE), PBE0, and HSE03 functionals. $d_{12}$ is the interlayer distance (in Å) between the first and second topmost layers. Numbers in parentheses refer to the change (in %) relative to the theoretical interlayer bulk distance ($a_0/\sqrt{3}$). $E_{surf}$ is the average surface energy of the relaxed and unrelaxed sides of the slab, normalized to the (111) surface unit cell. In this and the following tables, calculations for the four layer thick slab using $6\times6\times1$ (structural properties) and $8\times8\times1$ (energetics) $k$-point grids are reported. All calculations were performed using a $c(2\times4)$ surface unit cell.

| | $d_{12}$ (Å) | $E_{surf}$ [eV/(111) unit cell] |
|---|---|---|
| | Cu | |
| LDA | 2.01 (−0.9%) | 0.588 |
| PBE | 2.08 (−0.9%) | 0.455 |
| PBE0 | 2.06 (−1.8%) | 0.465 |
| HSE03 | 2.08 (−0.9%) | 0.453 |
| B3LYP (Ref. 28) | 2.11 (−1.2%) | 0.500 |
| | Rh | |
| LDA | 2.13 (−1.6%) | 1.006 |
| PBE | 2.17 (−1.6%) | 0.814 |
| PBE0 | 2.17 (−0.6%) | 0.849 |
| HSE03 | 2.16 (−1.0%) | 0.845 |
| | Pt | |
| LDA | 2.26 (+0.4%) | 0.813 |
| PBE | 2.30 (+0.7%) | 0.618 |
| PBE0 | 2.30 (+1.3%) | 0.644 |
| HSE03 | 2.30 (+1.3%) | 0.672 |
| B3LYP (Ref. 27) | 2.39 (+2.1%) | 0.517 |

The calculated LDA surface energies compare well with previous calculations.[49] The GGA surface energy is 0.45, 0.81, and 0.62 eV for Cu, Rh, and Pt, respectively, also in agreement with the values reported in the literature (0.50, 0.81, and 0.65 eV).[27,50,51] The PBE0 and HSE03 functionals give a slightly increased surface energy compared to the PBE functional. Such an increase of the surface energies is pointing toward an improved description using the hybrid functionals, but they are still underestimated compared to experiments: the experimental surface energies are ~0.65 eV for Cu(111), ~1.08 eV for Rh(111), and ~1.08 eV for Pt.[52] The B3LYP results[27,28] do not follow a consistent trend, with an increased surface energy for Cu and a decreased one for Pt. We have also calculated the PBE and HSE03 work function for the three (111) metal surfaces (not shown in Table II). For Cu, we have 6.34 (6.10) eV, for Rh, 5.38 (5.05) eV, and for Pt, 5.69 (5.64) eV using the PBE (HSE03) functional. The experimental values are 4.98, 4.98, and 5.65 eV for Cu, Rh, and Pt.[53] We note that PBE values are overestimated compared to experimental values; the HSE03 functional reduces the overestimation and gives better agreement with experiments especially for Rh and Pt.

Finally, for the CO molecule, the calculated bond length ($d_{CO}$) is 1.135, 1.143, 1.133, and 1.131 Å for LDA, GGA

TABLE III. Relevant structural parameters and energetics of CO on the Cu(111) surface (top, fcc, and hcp sites) using the LDA, GGA (PBE), PBE0, and HSE03 functionals (all the distance in Å). $d_{C\text{-}O}$ is the vertical distance between C and O, and in parentheses the relative variation with respect to the theoretical value of the free CO molecule (%) is given; $d_{C\text{-}X}$ is defined as the *minimum* height difference between the $z$ coordinate of the C and metal atom directly involved in the C-$X$ bonds; buckling $b$ is the distance between the outermost and the innermost metal atom in the first layer; $d_{12}$ is the mean change (%) of the distance between the first and second layers with respect to the theoretical value of the bare unrelaxed surface; $E_{ads}$ is the adsorption energy in eV. The preferred site (and corresponding adsorption energy) is written in boldface.

| Method | Site | $d_{C\text{-}O}$ (Å) | $d_{C\text{-}X}$ (Å) | $b$ (Å) | $d_{12}$ (%) | $E_{ads}$ (eV) |
|---|---|---|---|---|---|---|
| LDA | top | 1.149 (+1.2%) | 1.798 | 0.088 | −1.0 | −1.286 |
| | **fcc** | 1.174 (+3.5%) | 1.355 | 0.094 | +0.5 | **−1.660** |
| | hcp | 1.174 (+3.5%) | 1.360 | 0.068 | +0.4 | −1.642 |
| PBE | top | 1.158 (+1.3%) | 1.844 | 0.124 | −1.2 | −0.709 |
| | **fcc** | 1.183 (+3.5%) | 1.395 | 0.109 | +0.5 | **−0.874** |
| | hcp | 1.182 (+3.4%) | 1.399 | 0.082 | +0.6 | −0.862 |
| PBE0 | **top** | 1.144 (+0.9%) | 1.856 | 0.138 | −1.7 | **−0.606** |
| | fcc | 1.163 (+2.6%) | 1.425 | 0.135 | +0.7 | −0.579 |
| | hcp | 1.161 (+2.5%) | 1.450 | 0.105 | +0.7 | −0.565 |
| HSE03 | **top** | 1.142 (+1.0%) | 1.864 | 0.146 | −1.7 | **−0.561** |
| | fcc | 1.160 (+2.6%) | 1.417 | 0.143 | +0.7 | −0.555 |
| | hcp | 1.158 (+2.4%) | 1.413 | 0.099 | +1.2 | −0.535 |

(PBE), PBE0, and HSE03, close to the values reported by Neef and Doll (1.150 and 1.140 Å using PW91 and B3LYP[28]). The experimental bond length is 1.128 Å.[54] As far as the HOMO-LUMO gap is concerned, we find 6.80, 6.90, 10.60, and 8.80 eV using LDA, GGA (PBE), PBE0, and HSE03, respectively. The hybrid functionals give an energy gap increased by ~2–3 eV due to the downshift of the HOMO and a simultaneous upshift of the LUMO. The negative of the calculated HOMO energy is 9.0, 8.6, 10.6, and 10.0 eV using LDA, GGA (PBE), PBE0, and HSE03, respectively, compared to the experimental ionization potential of 14.10 eV.[55]

## IV. CO ADSORPTION: ENERGETICS AND STRUCTURAL PROPERTIES

In Tables III, IV, and V, we show the results for the adsorption of a CO molecule on Cu, Rh, and Pt surfaces, respectively. As expected, using the standard LDA and GGA functionals, the wrong site is preferred (shown in boldface), namely, fcc, hcp, and fcc for Cu, Rh, and Pt, in agreement with previous calculations.[27,28,56] The order of the sites with respect to the energy (starting from the most stable one) is fcc, hcp, top for Cu, hcp, fcc, top for Rh, and fcc, hcp, top for Pt. These site orders generally agree with those reported in Refs. 27, 28, and 56, although different surface reconstructions and computational methods were used. It should be noted that, for the Cu case, our calculated adsorption energy for the most stable site is lower by more than 400 meV compared to that given in Ref. 28. Also, the surface energy (bare surface) differs (see the previous section). These discrepancies can be possibly related to the different computational method used in Ref. 28, where a local basis set has been applied.

Using PBE0 or HSE03, the top site is preferred for Cu and Rh, in agreement with experiment. For Cu and PBE0 and HSE03, the site order is top, fcc, hcp (the same as found in Ref. 28 using B3LYP). The calculated adsorption energy (top site) is about −0.60 eV. This value is also close to that reported in Ref. 28 (−0.57 eV). The relative energy splitting ($\Delta E$) between hcp and top is ~40 meV using PBE0 and ~30 meV using HSE03. A larger energy splitting (150 meV) was found by Neef and Doll,[28] and an even larger one (~200 meV) in Ref. 12 using B3LYP. Furthermore, we find an almost degeneracy between the top and fcc sites using HSE03 ($\Delta E = \sim 6$ meV).

For Rh, the site order is top, hcp, fcc using both hybrid functionals. The calculated adsorption energy is −2.109 eV and −2.012 eV using PBE0 and HSE03. The splitting top-fcc is only ~5 meV using PBE0 and ~16 meV using HSE03, hence certainly within the error bars of the present calculations. Therefore, even though the calculated adsorption energies predict the correct site order for Cu and Rh, we can only safely conclude that the applied hybrid functionals reduce the tendency of LDA and GGA functionals to favor the hollow site with respect to the top site.

Finally, for Pt, neither PBE0 nor HSE03 recovers the correct site preference: the top site remains unfavored with respect to the fcc site, and the top and hcp sites are almost degenerate within the numerical accuracy. We, however, note that the top-fcc energy difference is ~350 meV (LDA), ~160 meV (GGA), ~56 meV (PBE0), and ~70 meV

TABLE IV. Relevant structural parameters and energetics of CO on the Rh (111) surface (top, fcc, and hcp sites) using the LDA, GGA (PBE), PBE0, and HSE03 functionals. See caption of Table III for details.

| Method | Site | $d_{C\text{-}O}$ (Å) | $d_{C\text{-}X}$ (Å) | $b$ (Å) | $d_{12}$ (%) | $E_{ads}$ (eV) |
|---|---|---|---|---|---|---|
| LDA | top | 1.155 (+1.8%) | 1.810 | 0.167 | +0.0 | −2.480 |
| | fcc | 1.185 (+4.5%) | 1.350 | 0.083 | +1.0 | −2.733 |
| | **hcp** | 1.187 (+4.6%) | 1.330 | 0.083 | +0.8 | **−2.801** |
| PBE | top | 1.165 (+1.9%) | 1.827 | 0.213 | +0.3 | −1.870 |
| | fcc | 1.195 (+4.5%) | 1.379 | 0.082 | +0.9 | −1.906 |
| | **hcp** | 1.197 (+4.7%) | 1.348 | 0.096 | +1.3 | **−1.969** |
| PBE0 | **top** | 1.149 (+1.4%) | 1.834 | 0.234 | +2.5 | **−2.109** |
| | fcc | 1.185 (+4.6%) | 1.330 | 0.048 | +2.8 | −2.024 |
| | hcp | 1.185 (+4.6%) | 1.344 | 0.118 | +4.3 | −2.104 |
| HSE03 | **top** | 1.152 (+1.8%) | 1.811 | 0.172 | +0.4 | **−2.012** |
| | fcc | 1.193 (+5.5%) | 1.351 | 0.063 | +1.9 | −1.913 |
| | hcp | 1.191 (+5.3%) | 1.342 | 0.100 | +2.2 | −1.996 |

(HSE03). Therefore, the tendency to favor the hollow sites is again reduced using hybrid functionals, but not sufficiently so for Pt. In order to rule out possible errors due to the $k$-point mesh, we performed additional calculations for the HSE03 case and CO on Pt using a $12\times12\times1$ $k$-point grid and downsampling the HF exchange part to $6\times6\times1$ $k$ points. We found that the relative stability of the top and fcc sites changed by only ~20 meV. Also, increasing the number of layers to 6 did not change the site order. The presented numbers are thus essentially converged.

Finally, we compare the calculated adsorption energies of Cu, Rh, and Pt with experimental values. For Cu(111), the experimental values are in the range from −0.52 to −0.46 eV,[57,58] close to our calculated value (≈−0.60 eV). For Rh(111), they are between −1.65 and −1.43 eV.[59,60] In this case, the theoretical values are too large by ~0.40–0.60 eV and, worse, the hybrid functionals give a slight increase of the adsorption energy compared to the gradient corrected functional. This result is certainly disappointing, and we will return to it in the Conclusions. For Pt(111), experimental values are in the range from −1.71 to −1.43 eV,[6,61,62] which compare reasonably well with the PBE value. Again, the hybrid functionals clearly worsen the agreement with experiment.

Concerning the geometry relaxations, we summarize the trend common to all four functionals: (i) The CO bond length is slightly elongated with respect to the theoretical value for the isolated molecule ($d_{CO}$=1.14 Å) in the top site, and even more so in the hollow sites. This holds for all three metal surfaces. (ii) The elongation of $d_{CO}$ correlates with a corre-

TABLE V. Relevant structural parameters and energetics of CO on the Pt (111) surface (top, fcc, and hcp sites) using the LDA, GGA (PBE), PBE0, and HSE03 functionals. See caption of Table III for details.

| Method | Site | $d_{C\text{-}O}$ (Å) | $d_{C\text{-}X}$ (Å) | $b$ (Å) | $d_{12}$ (%) | $E_{ads}$ (eV) |
|---|---|---|---|---|---|---|
| LDA | top | 1.149 (+1.2%) | 1.827 | 0.186 | +0.5 | −2.251 |
| | **fcc** | 1.184 (+4.3%) | 1.329 | 0.130 | +2.5 | **−2.601** |
| | hcp | 1.183 (+4.2%) | 1.314 | 0.132 | +2.0 | −2.576 |
| PBE | top | 1.158 (+1.3%) | 1.839 | 0.227 | +0.5 | −1.659 |
| | **fcc** | 1.194 (+4.4%) | 1.329 | 0.132 | +2.3 | **−1.816** |
| | hcp | 1.194 (+4.4%) | 1.324 | 0.149 | +2.4 | −1.750 |
| PBE0 | top | 1.142 (+0.8%) | 1.818 | 0.237 | +0.8 | −1.941 |
| | **fcc** | 1.177 (+3.9%) | 1.304 | 0.215 | +3.2 | **−1.997** |
| | hcp | 1.180 (+4.1%) | 1.291 | 0.226 | +2.6 | −1.944 |
| HSE03 | top | 1.143 (+1.1%) | 1.821 | 0.200 | +0.5 | −1.793 |
| | **fcc** | 1.177 (+4.1%) | 1.320 | 0.177 | +3.3 | **−1.862** |
| | hcp | 1.177 (+4.1%) | 1.330 | 0.177 | +2.2 | −1.808 |

TABLE VI. Dependence of the site order on the sampling of the surface Brillouin zone using hybrid functionals and the PBE functional. Energies are referenced to the top site. PBE0 results are evaluated using the full $k$-point grid; HSE03 results are evaluated using the reduced as well as the full grid (numbers in parentheses) for the nonlocal exchange (see text for details).

| | PBE0 | | HSE03 | | PBE | |
|---|---|---|---|---|---|---|
| | fcc | hcp | fcc | hcp | fcc | hcp |
| | | | Cu | | | |
| $4\times4\times1$ | 0.095 | 0.097 | 0.099 (0.086) | 0.106 (0.094) | −0.097 | −0.089 |
| $6\times6\times1$ | −0.029 | −0.004 | −0.019 (−0.024) | 0.010 (0.003) | −0.175 | −0.158 |
| $8\times8\times1$ | 0.027 | 0.041 | 0.006 (0.006) | 0.026 (0.028) | −0.165 | −0.153 |
| | | | Rh | | | |
| $4\times4\times1$ | 0.099 | 0.000 | 0.079 (0.081) | −0.006 (−0.022) | −0.040 | −0.105 |
| $6\times6\times1$ | 0.118 | −0.007 | 0.076 (0.074) | 0.005 (−0.003) | −0.067 | −0.130 |
| $8\times8\times1$ | 0.085 | 0.005 | 0.089 (0.094) | 0.016 (0.048) | −0.061 | −0.131 |
| | | | Pt | | | |
| $4\times4\times1$ | 0.047 | −0.027 | −0.091 (−0.112) | −0.045 (−0.062) | −0.127 | −0.106 |
| $6\times6\times1$ | −0.073 | 0.067 | −0.062 (−0.070) | −0.011 (−0.014) | −0.118 | −0.094 |
| $8\times8\times1$ | −0.056 | −0.003 | −0.069 (−0.069) | −0.015 (−0.015) | −0.121 | −0.095 |

sponding contraction of $d_{C-X}$ from low-coordination (top) to high-coordination sites (fcc, hcp). (iii) The buckling $b$ is larger for the top site. (iv) $\Delta d_{12}$ varies significantly from top to hcp sites, especially for Cu, where an inward relaxation for atop adsorption and an outward relaxation for the hollow sites are observed, whereas an outward relaxation is found in all three sites for Rh and Pt.

We conclude this section with a brief discussion of the $k$-point convergence presented in Table VI. Concentrating first on the PBE functional, we note that $k$-point convergence is slowest for the Cu surface, but fairly fast for the other two systems. A relative precision of 10 meV can be attained using $6\times6\times1$ $k$ points for all three systems [sampling specified for $c(2\times4)$ supercell]. The $4\times4\times1$ $k$-point set results in errors between 80 meV (Cu), 30 meV (Rh), and 10 meV (Pt). The HSE03 functional shows a similar convergence rate, with errors being only slightly larger. Now, $6\times6\times1$ $k$ points are sufficient to yield energies to within a precision of 15 meV, whereas the $4\times4\times1$ $k$-point grid causes errors between 120 meV (Cu) and 30 meV (Rh and Pt). Reducing the $k$-point sampling for the presentation of the nonlocal Fock exchange part has only a very small effect on the relative energies (10 meV), which is more than acceptable, in particular, in view of a speed up by a factor 4 if the sampling for the nonlocal part of the Hamiltonian is reduced in the $x$ and $y$ directions by a factor 2.

The PBE0 functional, however, converges exceedingly slowly, with discrepancies between $6\times6\times1$ and $8\times8\times1$ $k$ points being up to 50 meV. We were unable to increase the $k$-point grid beyond $8\times8\times1$ points with our available computational resources, but the relative energies using $8\times8\times1$ $k$ points are typically within 10–20 meV of those obtained using the HSE03 functional, and we expect them to come even closer to the HSE03 results, if the $k$-point set were further improved. This clearly demonstrates that the HSE03 functional is vastly superior in terms of computational requirements, in particular, for metallic systems. The calculations using the HSE03 functional and $6\times6\times1$ $k$ points with the Hartree-Fock part presented on a $3\times3\times1$ $k$-point grid are typically a factor 12 faster than the PBE0 calculations using $8\times8\times1$ $k$ points, although both yield practically the same results.

## V. ELECTRONIC PROPERTIES

According to the Blyholder model,[63] the interaction of the CO molecule with a transition-metal surface is usually described as the sum of two contributions. The first is due to the overlap of the HOMO $5\sigma$ with metal states. Since this interaction is accompanied by donation of electrons from the $5\sigma$ orbital into empty metal surface orbitals, this term is called donating term. The second term is due to the interaction of the surface-electron bands with the LUMOs $2\pi^*$. This is a back-donating term, since now electrons are transferred from the metal surface orbitals into the $2\pi^*$ orbitals. This simplistic model has been refined by Föhlisch *et al.*[64,65] using x-ray emission spectroscopy and *ab initio* cluster calculations. They showed that the $\pi$ bonding is manifested through the creation of a $d_\pi$ complex related to a hybridization of $1\pi$ and $2\pi^*$ orbitals with metal states. The $4\sigma$ and $5\sigma$ orbitals and the metal states form a hybrid $d_\sigma$ band. The work of Föhlisch *et al.* concentrates mainly on the interaction of the frontier orbitals with metal $d$ states; however, another often overlooked issue is that CO chemisorption to a transition-metal surface also involves interactions between the broad metal $sp$ valence electron band (which contains approximately one electron per atom for Cu, Rh, and Pt) and the CO orbitals. Due to symmetry, the $2\pi^*$ orbitals cannot interact with the $s$ or $p_z$ orbitals for top site adsorption, but the $2\pi^*-sp_z$ interaction is strong at high-coordination sites,

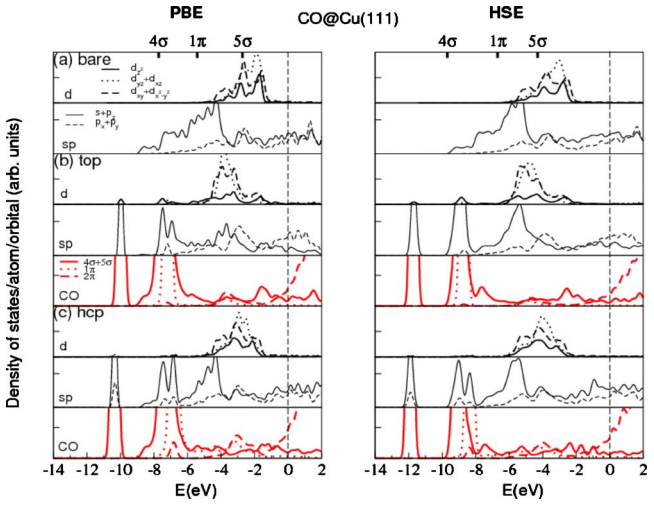


FIG. 1. (Color online) Orbital resolved electronic DOSs for the topmost Cu layer of the bare surface [panels (a)-d and (a)-sp] and for CO adsorbed at the top [panels (b)-d, (b)-sp, and (b)-CO] and hcp hollow sites [panels (c)-d, (c)-sp, and (c)-CO]. The DOSs are projected onto the metal $d$ states [panels (a)-d, (b)-d, and (c)-d: continuous, dotted, and dashed thick lines correspond to $d_{z^2}$, $d_{yz}+d_{xz}$, and $d_{xy}+d_{x^2-y^2}$ DOS, respectively], onto metal $sp$ states [panels (a)-sp, (b)-sp, and (c)-sp: continuous and dashed thin lines correspond to $s+p_z$ and $p_x+p_y$ DOS, respectively], and onto molecular orbitals [panels (b)-CO and (c)-CO: continuous, dotted, and dashed thick red lines correspond to $4\sigma+5\sigma$, $1\pi$, and $2\pi^*$ DOS, respectively]. The Fermi level is located at 0 eV. In panel (a)-d, we show the one-electron energies of the $4\sigma$, $1\pi$, and $5\sigma$ molecular levels aligned with the Fermi level using bold tick marks.

since *antisymmetric* combinations of surface $sp_z$ orbitals are available at these sites.[66]

In order to gain insight on the effect of hybrid functionals on the electronic properties, we show the orbital resolved electronic density of states (DOS) for the Cu, Rh, and Pt surfaces in Figs. 1, 2, and 3, respectively. For each figure, we show the DOS for the bare surface layer [(a), panels d, sp], for CO adsorbed on the top [(b), panels d, sp, CO], and hollow site [(c), panels d, sp, CO] as obtained using PBE (left column) and HSE03 (right column). Here, d, sp, and CO indicate the projection onto $d$ and $sp$ metal states and CO molecular orbitals, respectively. In panel (a)-d, we show the one-electron energies of the $4\sigma$, $1\pi$, and $5\sigma$ molecular levels aligned with the Fermi level using bold tick marks.[67]

Since there are no principal differences between the PBE0 and HSE03 DOS, only results for the latter are shown. We caution the reader that the following analysis based on the atom-projected DOS can only give qualitative insight on variations of the chemisorption energies upon changing the adsorption sites, the metal surface, and the exchange-correlation functional. A more powerful and quantitative analysis can be done by using the concept of *surface group orbitals* introduced by van Santen,[68–70] but this is beyond the purpose of this paper.

We recall the basic features of the interaction of the CO molecule with the metal surface,[3,66,71,72] and we first focus on the PBE DOS for the Cu case (Fig. 1, left column). From

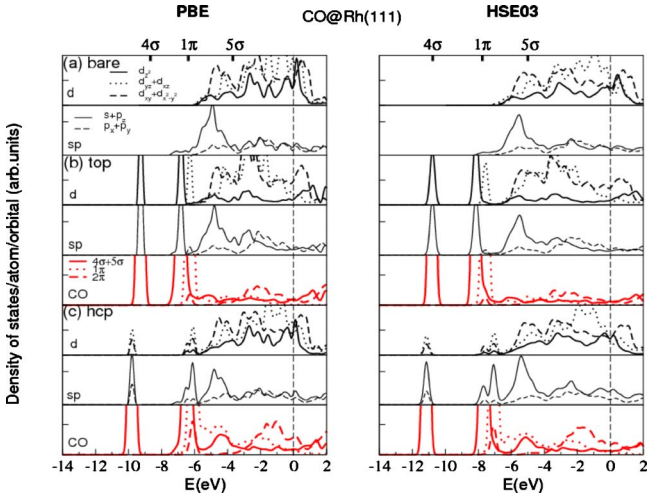


FIG. 2. (Color online) Orbital resolved electronic DOS (a) for the topmost Rh layer of the bare surface and for CO adsorbed at the (b) top and hcp (c) hollow site. See caption of Fig. 1 for details.

panels (a)-d and (a)-sp, we note that the Cu $d$ band is *almost* completely filled and is centered around $\epsilon_d \sim -2.4$ eV ($d$ band center of gravity) with $\delta\epsilon_d = 1.52$ eV ($d$ band width);[73] the $sp$ band extends over a larger energy range below the Fermi energy, but it is strongly peaked around −5 eV; the $5\sigma$ level is located at $\sim -2.70$ eV, and the $2\pi^*$ level is positioned at $\sim 4.20$ eV above the Fermi energy.

Let us now consider the interaction of the metal states with the CO $\sigma$ orbitals in the top configuration [Fig. 1(b)]. The metal $d$ bands broaden and shift down to lower energies due to the interaction with the CO molecule [compare panel (b)-d with panel (a)-d]. In particular, the $d_{z^2}$ DOS is strongly modified. In panel (b)-CO, we see that the $4\sigma$ and $5\sigma$ orbitals are shifted to lower energy (two main peaks at −10 and −7 eV with continuous line). Comparing panels in (b), it is clear that a strong interaction between $d_{z^2}$ and $sp_z$ metal states and the $\sigma$ molecular states takes place, giving rise

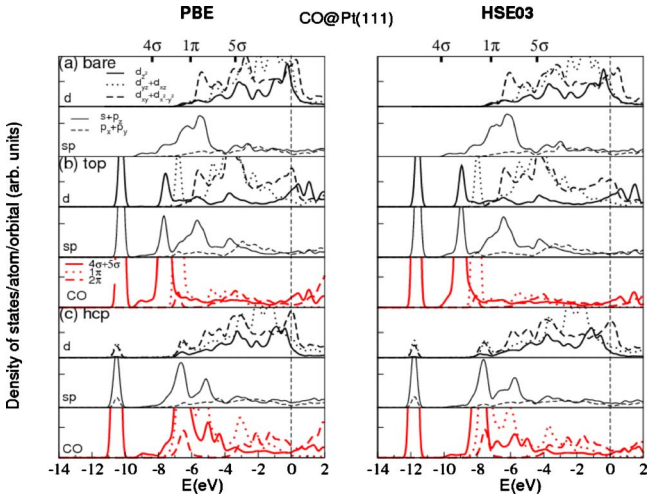


FIG. 3. (Color online) Orbital resolved electronic DOS (a) for the topmost Pt layer of the bare surface and for CO adsorbed at the (b) top and hcp (c) hollow site. See caption of Fig. 1 for details.

to a bonding contribution below the Fermi level (below ~−6 eV) and nonbonding and antibonding contributions partly even above the Fermi level ($d_\sigma$ band).[64,66] We recall that since almost fully occupied states are interacting, the interaction would be only a Pauli-like repulsion, if the antibonding $\sigma$-$d_{z^2}$ hybrid states were not pushed above the Fermi level (relief of Pauli repulsion).[74] The corresponding depletion of $5\sigma$ states (donation from CO to the metal) is in accordance with the Blyholder model.

Let us now consider the $\pi$ orbitals. In panel (b)-CO, we note that they are shifted to lower energy due to the interaction with $d_{yz}$, $d_{xz}$, and $p_x p_y$ metal states (bonding contribution). The $1\pi$ states are found at ~−7 eV (dotted line), and a small peak of $2\pi^*$ symmetry at the position of the $1\pi$ orbital is visible and related to the $1\pi$-$2\pi^*$ hybridization.[64] Above −6 eV, a nonbonding and antibonding $1\pi$-derived band develops ($d_\pi$ band)[64] which, however, remains below the Fermi energy (Pauli-like repulsion). The bonding states due to the interaction between the $2\pi^*$ orbital and the $d$ band are found around −4 eV (again $d_\pi$ complex)[64] and antibonding interactions well above the Fermi energy (not shown in the figure). The partial occupation of the $2\pi^*$ molecular orbital corresponds to a back donation of electrons from the substrate to the originally empty $2\pi^*$ molecular orbital, in accordance with the Blyholder model.

For the hcp site, there are some differences. The $d_{z^2}$ orbital is only marginally affected upon adsorption, whereas the $d_{yz}$ ($d_{xz}$) and $d_{xy}$ ($d_{x^2-y^2}$) bands are broadened and shifted to lower energy [compare panel (c)-d with panel (a)-d]. The interaction is mainly with the $\pi$ orbitals: the peaks with dashed and dotted lines above −6 eV in panel (c)-CO have increased compared to the corresponding ones in panel (b)-CO. In accordance with the arguments of Ref. 66, the interaction between the metal $s$ and $p$ states and the CO $\pi$ states is also enhanced, as reflected by a downshift of the metal $sp$ states. Note that three metal atoms are affected by adsorption in the hollow site as compared to one metal atom for the top site. In summary, the $\pi$-$d$ and $\pi$-$sp$ interaction is larger for the hcp site than for atop adsorption.

At this point, before considering the HSE03 DOS, we stress again that CO chemisorption to a transition-metal surface involves interaction of the molecular frontier orbitals and the broad $s$ and narrow $d$ band. The question whether the single-atom or high-coordination site is favored is clearly the result of a subtle balance between *single-atom* favoring interactions with the $5\sigma$ molecular states and *high-coordination* favoring interactions with the $2\pi^*$ molecular states. For CO on Cu(111), the balance between single-atom and high-coordination directing interactions is such that the hollow site adsorption is favoured for the PBE functional.

We now turn our attention to Fig. 1, right column. For the bare surface [(a)-d], we see that the $d$ states are shifted to lower energy by ~1 eV with respect to the Fermi level compared to the PBE DOS ($\epsilon_d$=−3.6 eV), but the overall spectral shape and the bandwidth remain almost unchanged. The downward shift of the HSE03 $d$ bands can be understood as a result of the reduction of the self-interaction within the $d$ shell in the hybrid functional formalism. It is also clearly seen that the occupied (unoccupied) molecular levels are shifted downward (upward) with respect to the Fermi energy: the $5\sigma$ level is now located at −4.30 eV and the $2\pi^*$ level is at 4.50 eV. The change of the energy positions of the noninteracting molecular levels with respect to the Fermi energy is mainly related to the increased HOMO-LUMO gap in the free molecule, and also partly caused by the reduced work function for the HSE03 functional (6.10 eV compared to 6.30 eV for PBE). The effect of the inclusion of part of the exact exchange on the broad $sp$ band is different. As a matter of fact, the $sp$ band is restrained to be located at the Fermi level (it is partially occupied), and the main effect of the nonlocal exchange is to increase the total bandwidth by 0.70 eV [compare left and right panel (a)-sp]. The above analysis immediately leads to a first conclusion. The downshift of the $d$ band and *simultaneous* upshift of the $2\pi^*$ levels suggest a reduced $2\pi^*$-$d$ interaction: according to second order perturbation theory, the larger energy distance between the unperturbed energy levels weakens the interaction. Inspection of the calculated DOS confirms this conjecture for HSE03: (i) the $d_\pi$ peaks are much weaker and (ii) hybridization between $2\pi^*$ and $1\pi$ molecular orbitals decreases corresponding to a *decrease* of the bonding interaction between the CO $\pi$ states and the metal $d$ states according to Föhlisch *et al.*[64]

We now summarize our analysis concerning the differences between the PBE and HSE03 functional. For the noninteracting fragments (bare surface and CO molecule), the HSE03 functional (i) pushes the occupied molecular levels down in energy, whereas the unoccupied molecular orbitals are moved up in energy, and (ii) the fully occupied $d$ band is shifted down in energy. We have seen that these two *combined* effects generally disfavor the $\pi$-*metal* interaction. It decreases for both the atop and the hollow site, but the destabilization is stronger in the hollow sites, in accordance with the observation that the $2\pi^*$ interaction is dominant at the hollow sites. This is confirmed by the observation that the adsorption energies in Table III decrease for both atop and hollow sites, but the effect is twice as strong for the hollow sites (compare the relative variation of the adsorption energies from PBE to HSE03, in Table III). A quantitative confirmation of this picture stems from the occupation of the $2\pi^*$ orbital in the hollow site. We recall that the larger the $2\pi^*$ occupation is, the stronger is the interaction of $2\pi^*$ with the metal states.[66] The $2\pi^*$ occupation is 0.80 and 0.66 electron using PBE and HSE03, respectively; hence, the occupation decreases by ~17% from PBE to HSE03.

Let us now consider the CO adsorbed on the Rh(111) surface in Fig. 2. In the following, we mainly concentrate on the differences between the PBE and HSE03 description (left and right panels). For the bare surface and HSE03 [panel (a)-d], there is a general downshift (upshift) of the occupied (unoccupied) part of the $d$ bands with respect to the Fermi energy. This leads to a small downshift of the center of gravity ($\epsilon_d$=−1.86 and −2.23 eV using PBE and HSE03) and a sizable larger bandwidth ($\delta\epsilon_d$=7.40 and 8.90 eV using the PBE and HSE03 functional). For atop adsorption [panel (b)-d], we see a small decrease of the intensity of the corresponding $d_\pi$ band [dotted line in panel (b)-CO]. There is also a small reduction of the $1\pi$ and $2\pi^*$ hybridization and of the $2\pi^*$-$d$ interaction (reduction of the intensity of the corresponding broad bands with dashed line). As far as the $\sigma$-$d$

interaction is concerned, one can see in panel (b)-CO that the $d_\sigma$ band is slightly less intense at the HSE03 level (reduction of the interaction strength). For the hcp site, we observe the same trends as for the top site.

Let us summarize again the differences between PBE and HSE03. As opposed to Cu, the *d* band is only slightly shifted downward, but possesses a much larger bandwidth (1.50 eV). As a result, the strength of the $\pi$-*d* interaction is only slightly reduced using HSE03: the reduction of the $\pi$-*d* interaction caused by the upshift of the $2\pi^*$ orbital is counteracted by the larger *d* band width of the metal using HSE03. This is corroborated by the $2\pi^*$ occupation for the hollow site, which changes only from 1.05 to 1.01 electrons (i.e., ~4%) going from PBE to HSE03. We recall that for copper, the variation was about 17%, i.e., much larger than for Rh. The *s* electrons are largely affected by the introduction of the nonlocal exchange. For the bare surface, HSE03 reduces the self-interaction within the *s* shell and moves them to lower energies. This suggests an enhancement of the back donation due to the interaction of the $2\pi^*$ states with antisymmetric linear combinations of metal *s* orbitals, which, we recall, is active only for the hollow site.[66] For Rh, the balance between atop- and hollow-directing interactions gives still a slight preference for atop adsorption using HSE03 (see Table III).

Finally, we turn our attention to Pt(111). Basically, we observe the same trends as for Rh using HSE03: a downshift of the *d* band center of gravity and a larger bandwidth is observed ($\epsilon_d$=−2.13 and −2.53 eV, $\delta\epsilon_d$=8.29 and 9.32 eV using PBE and HSE03, respectively). The work function changes only little (5.69 and 5.64 using PBE and HSE03). For both adsorption sites, there are only small changes in the DOS due to the introduction of exact exchange. In particular, for the hollow site, we note that the peak corresponding to the $2\pi^*$ and $1\pi$ hybridization has the same intensity for HSE03 and PBE [panel (c)-CO]. Also, the $d_\pi$ intensity is almost the same as in the PBE case [panel (c)-CO, dashed line] as confirmed by the $2\pi^*$ occupation: it is 1.03 and 0.97 electrons using PBE and HSE03. That is, it decreases by only 6% using HSE03. Probably, the most pronounced difference between the 4*d* Rh and 5*d* Pt metal is the enhanced *s* occupation, related to the stronger binding of the 6*s* electrons (the shell structure requires that the orbitals are filled in the order 6*s*, 4*f*, 5*d*, 6*p*, placing the 6*s* electrons at significantly larger binding energies than 5*s* electrons). This effect is further enhanced by the HSE03 functional. As before, this should stabilize the CO in the hollow site due to the increased $\pi$-*s* interaction. Indeed, now the destabilization of the $\pi$-*d* interaction in the hollow site is not sufficient to yield the top site as preferred adsorption site.

## VI. DISCUSSION

Let us start with a brief discussion of the computational aspects of the current work. We have shown that periodic slab calculations using hybrid Hartree-Fock density functionals are perfectly feasible for metallic systems using a plane wave basis set. We have also shown that the HSE03 functional, suggested by Heyd *et al.*, yields practically identical results as the more conventional PBE0 functional, albeit at a computational cost that is reduced by about a factor of 10. This is achieved by replacing the long-range part of the Fock exchange by its density functional approximation, leading to a rapid *k*-point convergence of the nonlocal exchange and total energies. Thus, the HSE03 functional presents a promising functional for large scale studies of molecules on surfaces.

Our study concentrated on the chemisorption of the CO molecule on *d*-metal surfaces, specifically Cu(111), Rh(111), and Pt(111). The study has been pursued using local and generalized gradient density functionals and PBE0 and HSE03 hybrid Hartree-Fock density functionals. As expected, the LDA and GGA functionals give the wrong site preference for Cu, Rh, and Pt. In contrast, the PBE0 and HSE03 functionals reduce this tendency, predicting the correct site order for CO on Cu(111) and Rh(111). In both cases, the fcc and hcp sites are destabilized by roughly 150 meV compared to the top site. Unfortunately, the HSE03 and PBE0 functionals do not work so well for Pt(111), where the destabilization is only 50 meV for the fcc site and 80 meV for the hcp site, which is not sufficient to yield the correct site preference. In both Rh and Pt, we have made significant effort applying, for instance, different PAW sets and parameters (not all have been discussed in detail) to make certain that the present numbers are essentially converged within the theoretical framework.

The wrong site order for Pt is not the only unsatisfactory aspect of our study; results for the energetics are also largely disappointing. It is well accepted that gradient corrected functionals have a tendency to overestimate adsorption energies on metal surfaces.[2,75] One would have hoped that admixing a certain fraction of the exact nonlocal exchange lifts this deficiency, but this hope is not fulfilled by the PBE0 and HSE03 functionals. In fact, Cu is the only case where the hybrid functionals improve the overall energetics. This is related to the upshift of the empty CO $2\pi^*$ orbital and a simultaneous downshift of the filled Cu 3*d* states, with both effects reducing, in concert, the $2\pi^*$-*d* interaction; thus, the top site becomes preferred.

For Rh and Pt, the *d* band is restrained to stay at the Fermi level, and for the transition metals, the main effect of the inclusion of nonlocal exchange is an increase of the *d* band width. This increase of the *d* band width counteracts the reduced interaction caused by the upshift of the CO $2\pi^*$ orbital. One therefore observes that the interaction energies generally increase from PBE, over HSE03 to PBE0, with the last one yielding the largest *d* band width and the largest CO-metal interaction energies. In a ball pack, the increased metal band width caused by the nonlocal exchange is the main origin of problems: it partially restores the CO $2\pi^*$-*d* interaction that we had aimed to reduce by means of the hybrid functional. This counterbalance works efficiently for Pt, which has the largest *d* band width and the largest interaction matrix elements between molecule and metal states.[76] We also qualitatively argued that further contributions in favor of restoring the back-donative interaction may come from an enhanced interaction of $2\pi^*$ states at the hollow site with antisymmetric combination of *s* metal states,[66] but our analysis is not able to quantify and separate *s* and *d* contributions.

Unfortunately, there are reasons to believe that the inclusion of a significant fraction of the nonlocal exchange and the concomitant increase of the *d* band width in transition metals is the wrong physics. We have already commented on this issue in our recent work:[31] the analogy between *GW* and hybrid functionals suggests that the amount of nonlocal exchange should be chosen system dependent, applying more Hartree-Fock-like exchange in exchange dominated systems such as molecules and large gap insulators. In metals, on the other hand, the nonlocal exchange term in *GW* is almost entirely screened by the other electrons, so that the Coulomb hole term—corresponding to a local potential—becomes dominant. In metals, the proper description thus involves only a very weak screened-exchange interaction and the semilocal density functional approximation should do a perfectly adequate job. The same conclusion is reached using the adiabatic connection fluctuation dissipation theorem.[23] In a forthcoming paper,[77] we will present results of hybrid functional calculations of CO adsorption extended to other systems representative of 4*d* and 5*d* metal surfaces, including the B3LYP functional. Unfortunately, also in this case, the results are generally discomforting, suggesting that previous reports on the successful prediction of adsorption energies using B3LYP have to be considered with suspicion.

We are thus left with the intriguing problem of how to treat two disparate systems using the same unified theoretical footing. It is difficult to imagine that a hybrid functional with a fixed amount of nonlocal exchange is going to do the job. On passing, we also reiterate another result for hybrid functionals from Ref. 31: the exchange splitting in transition metals is significantly overestimated, resulting in too small atomization energies (found here as well for Pt) and a large overestimation of the magnetic moment in itinerant magnetic transition metals.

## VII. CONCLUSIONS

We conclude that although hybrid functional calculations for metals and metal surfaces are perfectly feasible, the results are by no means entirely satisfactory. The agreement with experiment is improved for CO on Cu(111), but the results are only marginally improved for CO on Rh(111) (correct site order but much too large adsorption energies) and hardly improved for CO on Pt(111) (wrong site order and too large adsorption energies). We have argued that this failure is related to the inclusion of nonlocal exchange in the metal slab, which results in an incorrect description of the metal bandwidth.

## ACKNOWLEDGMENT

This work was supported by the Austrian *Fonds zur Förderung der wissenschaftlichen Forschung*.

*alessandro.stroppa@univie.ac.at

[1] G. A. Somorjai, *Introduction to Surface Chemistry and Catalysis* (Wiley, New York, 1994).
[2] P. J. Feibelman, B. Hammer, J. K. Nørskov, F. Wagner, M. Scheffler, R. Stumpf, R. Watwe, and J. Dumesic, J. Phys. Chem. B **105**, 4018 (2001).
[3] G. Kresse, A. Gil, and P. Sautet, Phys. Rev. B **68**, 073401 (2003).
[4] M. Mavrikakis, J. Rempel, J. Greeley, L. B. Hansen, and J. K. Nørskov, J. Chem. Phys. **117**, 6737 (2002).
[5] Baro and H. Ibach, J. Chem. Phys. **71**, 4812 (1979).
[6] H. Steininger, S. Lehwald, and H. Ibach, Surf. Sci. **123**, 264 (1982).
[7] G. S. Blackman, M. L. Xu, D. F. Ogletree, M. A. Van Hove, and G. A. Somorjai, Phys. Rev. Lett. **61**, 2352 (1988).
[8] Y. Gauthier, M. Schmid, S. Padovani, E. Lundgren, V. Bus, G. Kresse, J. Redinger, and P. Varga, Phys. Rev. Lett. **87**, 036103 (2001).
[9] H. Orita, N. Itoh, and Y. Inada, Chem. Phys. Lett. **384**, 271 (2004).
[10] R. A. Olsen, P. H. T. Philipsen, and E. J. Baerends, J. Chem. Phys. **119**, 4522 (2003).
[11] B. Delley (private communication).
[12] Q.-M. Hu, K. Reuter, and M. Scheffler, Phys. Rev. Lett. **98**, 176103 (2007).
[13] A. Gil, A. Clotet, J. M. Ricart, G. Kresse, M. García-Hernández, N. Rösch, and P. Sautet, Surf. Sci. **530**, 71 (2003).
[14] S. E. Mason, I. Grinberg, and A. M. Rappe, Phys. Rev. B **69**, 161401(R) (2004).
[15] M. Gajdos and J. Hafner, Surf. Sci. **590**, 117 (2005).
[16] J. Paier, R. Hirschl, M. Marsman, and G. Kresse, J. Chem. Phys. **122**, 234102 (2005).
[17] W. Koch and M. C. Holthausen, *A Chemists' Guide to Density Functional Theory* (Wiley-VCH, Weinheim, 2001).
[18] E. R. Batista, J. Heyd, R. G. Hennig, B. P. Uberuaga, R. L. Martin, G. E. Scuseria, C. J. Umrigar, and J. W. Wilkins, Phys. Rev. B **74**, 121102(R) (2006).
[19] M. Ernzerhof and G. E. Scuseria, J. Chem. Phys. **110**, 5029 (1999).
[20] C. Adamo and V. Barone, J. Chem. Phys. **110**, 6158 (1999).
[21] A. D. Becke, J. Chem. Phys. **98**, 5648 (1993).
[22] C. Lee, W. Yang, and R. G. Parr, Phys. Rev. B **37**, 785 (1988).
[23] J. P. Perdew, M. Ernzerhof, and K. Burke, J. Chem. Phys. **105**, 9982 (1996).
[24] K. Burke, M. Ernzerhof, and J. P. Perdew, Chem. Phys. Lett. **265**, 115 (1997).
[25] K. Raghavachari, Theor. Chem. Acc. **103**, 361 (2000).
[26] J. Heyd, G. E. Scuseria, and M. Ernzerhof, J. Chem. Phys. **118**, 8207 (2003).
[27] K. Doll, Surf. Sci. **573**, 464 (2004).
[28] M. Neef and K. Doll, Surf. Sci. **600**, 1085 (2006).
[29] S. Chawla and G. A. Voth, J. Chem. Phys. **108**, 4697 (1998).
[30] G. Kresse and J. Furthmüller, Comput. Mater. Sci. **6**, 15 (1996).
[31] J. Paier, M. Marsman, K. Hummer, G. Kresse, I. C. Gerber, and J. G. Angyan, J. Chem. Phys. **124**, 154709 (2006).
[32] D. M. Ceperley and B. J. Alder, Phys. Rev. Lett. **45**, 566 (1980).
[33] J. P. Perdew, K. Burke, and M. Ernzerhof, Phys. Rev. Lett. **77**,

3865 (1996); **78**, 1396 (1997).
[34] P. E. Blöchl, Phys. Rev. B **50**, 17953 (1994).
[35] G. Kresse and D. Joubert, Phys. Rev. B **59**, 1758 (1999).
[36] M. Gajdos, A. Eichler, and J. Hafner, J. Phys.: Condens. Matter **16**, 1141 (2004).
[37] J. Heyd, G. E. Scuseria, and M. Ernzerhof, J. Chem. Phys. **124**, 219906 (2006).
[38] H. J. Monkhorst and J. D. Pack, Phys. Rev. B **13**, 5188 (1976).
[39] M. Methfessel and A. T. Paxton, Phys. Rev. B **40**, 3616 (1989).
[40] For details, see http://cms.mpi.univie.ac.at/vasp/
[41] V. N. Staroverov, G. E. Scuseria, J. Tao, and J. P. Perdew, Phys. Rev. B **69**, 075102 (2004).
[42] M. Sgroi, C. Pisani, and M. Busso, Thin Solid Films **400**, 64 (2001).
[43] J. J. Rehr, E. Zaremba, and W. Kohn, Phys. Rev. B **12**, 2062 (1975).
[44] J. Paier, M. Marsman, and G. Kresse, J. Chem. Phys. **127**, 024103 (2007).
[45] J. Wan, Y. L. Fan, D. W. Gong, S. G. Shen, and X. Q. Fan, Modell. Simul. Mater. Sci. Eng. **7**, 189 (1999).
[46] N. Materer, U. Starke, A. Barbieri, R. Doll, K. Heinz, M. A. van Hove, and G. A. Somorjai, Surf. Sci. **325**, 207 (1995).
[47] K. H. Chae, H. C. Lu, and T. Gustafsson, Phys. Rev. B **54**, 14082 (1996).
[48] A. Barbieri, M. van Hove, and G. A. Somorjai, in *The Structure Surfaces IV*, edited by X. D. Xie, S. Y. Tong, and M. A. van Hove (World Scientific, Singapore, 1994), p. 201.
[49] H. L. Skriver and N. M. Rosengaard, Phys. Rev. B **46**, 7157 (1992).
[50] J. F. Da Silva, C. Stampfl, and M. Scheffler, Surf. Sci. **600**, 703 (2006).
[51] L. Köhler (private communication).
[52] L. Vitos, A. V. Ruban, H. L. Skriver, and J. Kollár, Surf. Sci. **411**, 186 (1998).
[53] H. B. Michaelson, J. Appl. Phys. **48**, 4729 (1977).
[54] A. W. Mantz, J. K. G. Watson, K. N. Rao, D. L. Albritton, A. L. Schmeltekopf, and R. N. Zare, J. Mol. Spectrosc. **39**, 180 (1971).
[55] C.-G. Zhan, J. A. Nichols, and D. A. Dixon, J. Phys. Chem. A **107**, 4184 (2003).
[56] L. Köhler and G. Kresse, Phys. Rev. B **70**, 165405 (2004).
[57] P. Hollins and J. Pritchard, Surf. Sci. **89**, 486 (1979).
[58] M. K. Rose, T. Mitsui, J. Dunphy, A. Borg, D. F. Ogletree, M. Salmeron, and P. Sautet, Surf. Sci. **512**, 48 (2002).
[59] K. A. Peterlinz, T. J. Curtiss, and S. J. Sibener, J. Chem. Phys. **95**, 6972 (1991).
[60] M. J. P. Hopstaken and J. W. Niemantsverdriet, J. Chem. Phys. **113**, 5457 (2000).
[61] G. Ertl, M. Neumann, and K. M. Streit, Surf. Sci. **64**, 393 (1977).
[62] Y. Y. Yeo, L. Vattuone, and D. A. King, J. Chem. Phys. **106**, 392 (1997).
[63] G. J. Blyholder, J. Phys. Chem. **68**, 2772 (1964).
[64] A. Föhlisch, M. Nyberg, P. Bennich, L. Triguero, J. Hasselström, O. Karis, L. G. M. Pettersson, and A. Nilsson, J. Chem. Phys. **112**, 1946 (2000).
[65] A. Föhlisch, M. Nyberg, J. Hasselström, O. Karis, L. G. M. Pettersson, and A. Nilsson, Phys. Rev. Lett. **85**, 3309 (2000).
[66] R. A. van Santen and M. Neurock, *Molecular Heterogeneous Catalysis: A Conceptual and Computational Approach* (Wiley-VCH, Weinheim, 2005).
[67] The electronic molecular energies of the free CO molecule calculated in a large cube have the vacuum level as zero energy level. By adding the work function of the metal surface to the free molecular energy levels, the Fermi energy of the metal becomes the zero energy level.
[68] R. A. van Santen, J. Mol. Struct. **173**, 157 (1988).
[69] R. A. van Santen, J. Chem. Soc., Faraday Trans. 1 **83**, 1915 (1987).
[70] R. A. van Santen, Prog. Surf. Sci. **25**, 253 (1987).
[71] P. S. Bagus and G. Pacchioni, Surf. Sci. **278**, 427 (1992).
[72] R. Hoffmann, Rev. Mod. Phys. **60**, 601 (1988).
[73] The bandwidth and the center of gravity have been calculated isolating the *d* band intensity with a cutoff point chosen to lie at the point of maximum curvature in the upper leading shoulder of the DOS spectra in order to exclude spurious states projected out from the next *d* shell. This cannot be done in a fully unambiguous way. In any case, reasonable shifts of the cutoff point to higher energy affect the *d* band parameters in a negligible way.
[74] H. Aizawa and S. Tsuneyuki, Surf. Sci. **399**, L364 (1998).
[75] B. Hammer, L. B. Hansen, and J. K. Nørskov, Phys. Rev. B **59**, 7413 (1999).
[76] B. Hammer and J. K. Nørskov, Adv. Catal. **45**, 71 (2000).
[77] A. Stroppa and G. Kresse (unpublished).